Lidar thermometry using two-line atomic fluorescence

Malmqvist, E.; Borggren, J.; Aldén, M.; Bood, J.

Published in:
Applied Optics

DOI:
10.1364/AO.58.001128

2019

Document Version:
Publisher's PDF, also known as Version of record

applied optics

Lidar thermometry using two-line atomic fluorescence

E. Malmqvist,[1,*] J. Borggren,[2] M. Aldén,[1] and J. Bood[1]

[1]Division of Combustion Physics, Department of Physics, Lund University, Sölvegatan 14, Lund, Sweden
[2]Norsk Elektro Optikk Lund AB, Maskinvägen 1, Lund, Sweden
*Corresponding author: elin.malmqvist@forbrf.lth.se

Received 2 October 2018; revised 17 December 2018; accepted 2 January 2019; posted 4 January 2019 (Doc. ID 347062); published 31 January 2019

In this work, Scheimpflug lidar has been combined with the thermometric technique two-line atomic fluorescence, to carry out stand-off, spatially resolved temperature measurements. Indium atoms were seeded into a modified Perkin-Elmer-burner and two tunable single-mode diode lasers with their wavelengths tuned to 410.17 and 451.12 nm were used to excite the seeded atoms. The fluorescence signal was collected using both a line-scan detector and a two-dimensional intensified CCD camera. One-dimensional flame temperature profiles were measured at different heights above a porous-plug burner, located at a distance of 1.5 m from the lidar system. The technique was also used to demonstrate two-dimensional temperature measurements in the same flame. The accuracy of the measured temperature was found to be limited mainly by uncertainty in the spectral overlap between the laser emission and the indium atom absorption spectrum as well as uncertainty in laser power measurements. With the constraint that indium can be introduced into the measurement volume, it is anticipated that the developed measurement concept could constitute a valuable tool, allowing *in situ* spatially resolved thermometry in intractable industrial applications, sufferings from limited optical access, thus requiring remote single-optical-port sensing.

https://doi.org/10.1364/AO.58.001128

1. INTRODUCTION

A. Lidar

Diagnostics in large-scale combustion facilities, such as furnaces and industrial power plants, often requires a technique that can deliver range-resolved data over large distances with limited optical access. This makes many conventional diagnostic techniques used in combustion non-applicable in these environments since attainable probe volumes are relatively restricted and they require multiple and often spatially separated optical accesses. To be able to carry out practical diagnostics in these kinds of facilities, a measurement technique that is able to provide range-resolved measurements over long distances in the backwards direction is thus desired. The laser-based remote sensing method lidar (light detection and ranging) is a technique that fulfills these requirements. Conventional lidar techniques rely on pulsed lasers and time-of-flight detection to obtain range resolution. The pulse length and the bandwidth of the detector are thus the limiting factors for the achievable resolution. To be able to resolve the necessary spatial scales in most combustion environments, conventional lidar requires a laser pulse duration on the picosecond (ps) scale and a comparably fast detector. Lidar that utilizes ps pulses has been demonstrated for several combustion applications previously [1–4], where the highest range resolution demonstrated was ∼0.5 cm.

The Scheimpflug lidar method [5–7], used in this work, instead achieves range resolution by imaging a continuous-wave (CW) laser beam along the pixels of a one-dimensional (1D) or two-dimensional (2D) detector. Focus can be achieved along the laser beam at both close and far distances by placing the detector, the laser beam, and collection optics according to the Scheimpflug principle [8,9]. The range resolution, governed by the Scheimpflug principle, deteriorates with increasing distance from the detector, i.e., pixels observing the laser beam at far distances monitor a larger range interval than pixels observing the laser at close distances. The exact range scale and resolution is determined by the particular properties and arrangement of the collection optics, the size of the detector, and the width of the laser beam. For a more thorough description of the method, see [5,6,10]. The fact that this technique utilizes imaging instead of time-of-flight detection enables the use of small, robust, and less complex CW diode lasers and it opens up for high sampling rates. The feasibility of Scheimpflug lidar for combustion diagnostics, including achievable range coverage and resolution in a typical combustion setting, have been thoroughly discussed in [10]. The present work focuses on the implementation of two-line atomic fluorescence (TLAF) in a Scheimpflug lidar configuration for combustion thermometry.

B. Temperature Measurements

Temperature is one of the governing physical properties in combustion processes due to the strong exponential temperature dependence of chemical reaction rates, as generally described by the Arrhenius equation. Accurate and precise temperature measurements are thus essential in order to understand the combustion process and improve its efficiency. Reliable temperature measurements are also needed to calibrate other diagnostic studies, e.g., concentration measurements. A well-established laser-based thermometry technique for combustion studies is Rayleigh scattering, in which the temperature is extracted from the number-density dependence of the scattering intensity [11]. One of the advantages of this technique is the relatively low experimental complexity, making it relatively easy to perform 1D and 2D measurements. Unfortunately, the low Rayleigh scattering cross section of molecules together with the commonly present interference due to elastic scattering from surrounding surfaces and large particles limits the use of the technique. Another disadvantage is that the gas composition in the probe volume has to be known since the scattering cross section is different for different species.

Several thermometric techniques are based on probing the population distribution across two or more energy levels using one or several lasers. One such technique is coherent anti-Stokes Raman spectroscopy (CARS), which is a spectroscopic technique that provides temperature information with high accuracy and precision [12]. The temperature-dependent rotational or vibrational population of molecules is probed through a non-linear interaction with electromagnetic waves, i.e., high-intensity laser beams, and the resulting signal is a coherent beam, which upon spectrally dispersed detection reveals the vibrational and/or rotational distribution of the probed molecules. CARS has been used for point measurements for a long time and recent advances have made it possible to perform both 1D and 2D measurements [13,14]. In recent years, femtosecond and picosecond CARS have also been developed enabling kilohertz repetition rates and collision free measurements. The greatest disadvantage of CARS is the relatively high experimental and theoretical complexity [15].

Other spectroscopic thermometric techniques are based on detecting laser-induced fluorescence (LIF) from molecules. These techniques readily provide 1D and 2D measurements using naturally occurring species, such as OH and NO [16,17]. LIF can of course also be used in lidar but it is problematic to achieve a high spatial resolution using a traditional time-of-flight approach, since the time-of-flight detection scheme results in smearing of the signal in space due to the finite fluorescence lifetimes (of the order of nanoseconds at atmospheric pressure) of the probed species. Scheimpflug lidar has an advantage over time-of-flight lidar here since the finite fluorescence lifetime does not affect the range resolution [10]. Due to the low concentrations of the species, combined with their relatively low fluorescence yield, the resulting signal-to-noise ratios (SNRs) in LIF tend to be quite low. One technique that is able to improve on the SNR is TLAF [18–21]. In this thermometric technique the temperature-dependent difference in population between two fine structure levels in the electronic ground state of an atomic species is used to obtain the temperature. Atomic species, which typically have higher fluorescence yields than molecules, are introduced into the measurement volume and the populations in two states are probed by excitation to a common upper state, using two lasers, and then detecting the resulting fluorescence. The intensities of the fluorescence signals are proportional to the populations in the probed energy states, which in turn are governed by the temperature-dependent Boltzmann distribution. Temperature can thus be extracted from the ratio of the fluorescence signals. One advantage of this method is that the signal ratio is insensitive to spatial concentration differences. Temperature evaluation is done by comparing the measured ratio (R_{exp}) to simulated ratios. The experimental ratio is compensated for difference in laser power according to the following expression:

$$R_{\mathrm{exp}} = \frac{F_a/I_a}{F_b/I_b},$$

where I_a is the intensity of the laser light exciting atoms from level a, I_b is the intensity of the laser light exciting atoms from level b, F_a is the resulting fluorescence signal for excitation from a, and F_b is the resulting fluorescence signal for excitation from b. For more information about the evaluation method, see [21].

One of the great advantages of this thermometric technique is that the high signal strength of the fluorescence from atoms enables the use of CW diode lasers instead of high-power pulsed lasers, which in turn results in more compact, less complex, and robust experimental designs. This also means that the technique can easily be combined with Scheimpflug lidar to perform spatially resolved temperature measurements from the backward direction. In this work, we have carried out 1D and 2D TLAF temperature measurements in a flat, indium-seeded flame using Scheimpflug lidar. Section 2 describes the utilized equipment and experimental arrangement. The first part of Section 3 presents the results from range-resolved temperature measurement in a flame, and after that results showing an initial 2D temperature distribution are presented. The paper ends with conclusions and outlook in Section 4.

2. EXPERIMENTAL SETUP

The experimental setup is shown in Fig. 1. The measurements presented in this work were performed in a flat flame on a modified atomic-absorption burner (Perkin-Elmer) [22] with a stabilizer plate placed at the top of the flame. The porous plug of this McKenna-type burner has a diameter of 23 mm. The burner contains a nebulizer which seeds the flame with atoms using salt solutions containing the desired atoms. In these measurements, a methane/air flame, with equivalence ratio 1.2, was seeded with water-dissolved $InCl_3$ (0.03 M). Indium was selected as seeding species since it provides high temperature sensitivity at flame temperatures [21]. It should be noted though that other species, for example gallium, could be used if other temperature regimes are of interest. A 5 l/min co-flow of N_2 was used during the measurements. Two tunable, single-mode diode lasers (Toptica) were used to excite indium through the transitions $5^2P_{1/2} \rightarrow 6^2S_{1/2}$ at 410.17 nm and $5^2P_{3/2} \rightarrow 6^2S_{1/2}$ at 451.12. The resulting fluorescence at 451 nm was collected and registered by the detector. The results presented here were attained using either a line array

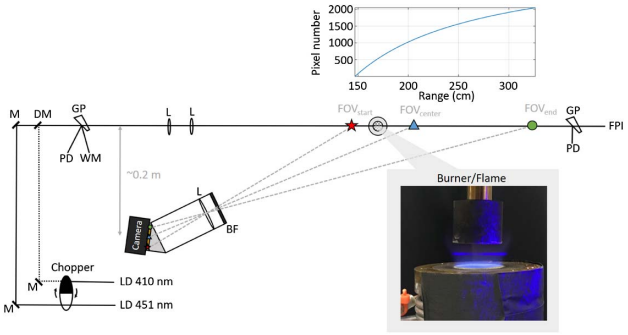

Fig. 1. Schematic experimental Scheimpflug lidar TLAF setup. GP, glass plate; PD, photodiode; LD, laser diode; M, mirror; DM, dichroic mirror; L, lens; FPI, Fabry–Perot etalon; WM, wavemeter; FOV, field-of-view. For practical combustion applications, the FPI could easily be placed with the other optical components close to the laser source. The figure also illustrates how Scheimpflug lidar achieves range resolution along the detector chip. The mean range of the start, center, and end pixels on the detector are marked with a star, triangle, and circle, respectively. The curve at the top of the figures shows the non-linear behavior of the range scale across the pixels of the detector. The example displayed here is for the case when the linear array detector is used. The gray insert shows a picture of the flame and the fluorescence signal.

camera, or a 2D intensified CCD (ICCD) camera (details presented in Table 1). A bandpass filter with a center wavelength of 450 nm and FWHM of 10 nm was placed in front of the collection lens ($f = 200$ mm) to suppress background interference.

The two laser beams were aligned with a chopper wheel, in such a way that a periodic switch between the laser sources and background (both beams blocked) could be performed. After the chopper wheel, the laser beams were overlapped using a dichroic mirror. The combined beams were sent through a glass plate and then focused with an $f = 1000$ mm lens resulting in a beam waist at the center of the flame at a distance of ~1.5 m from the detector. The two reflections obtained from the glass plate were aligned onto a wavemeter for wavelength monitoring and onto a photodiode for laser power calibration. The wavemeter was also used to perform an excitation scan with each laser to find the exact wavelength position of the peak of the absorption profiles. Figures 2(a) and 2(b) display these

Table 1. Specification of the Detectors Utilized in the Present Work

	Line Array	ICCD
Manufacturer	Synertronic Designs	Princeton Instruments
Model	Glaz-S	PI-MAX 4
Sensor type	CMOS	ICCD
Chip size (pixels)	1 × 2048	1024 × 1024[a]
Pixel Size (μm)	200 × 14	13 × 13
Sensitivity range (nm)	280–1000	350–950
Max readout rate (fps)	4000	7.7[b]

[a]282 × 1024 pixels were used during measurement.
[b]Refers to a configuration using all pixels and no binning.

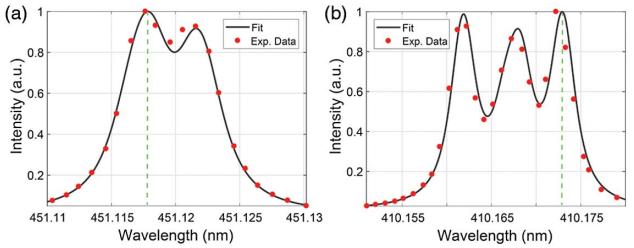

Fig. 2. Excitation scan on indium with excitation at transition (a) $5^2P_{3/2} \rightarrow 6^2S_{1/2}$ at 451.1 and (b) $5^2P_{1/2} \rightarrow 6^2S_{1/2}$ at 410.2 nm. The collected wavelength was at ~451.12 nm. The structures seen in the excitation scans are hyperfine structure. The excitation scans are used to calibrate what wavelength reading on the wavemeter corresponds to the peak of the absorption profile, so the laser wavelength can be chosen accordingly during the temperature measurements. The selected wavelengths for the transitions are marked with a dashed, vertical line.

high-resolution spectra, in which the hyperfine structure of the two transitions is clearly observable. The selected wavelengths for the transitions are marked with a dashed vertical line. Another glass plate was placed behind the burner which provided reflected laser light for another photodiode used for absorption measurements. A Fabry–Perot interferometer (FPI) was also placed behind the burner to verify that the lasers were operating in single-mode. For practical combustion applications, the FPI could easily be positioned together with the other optical components close to the laser source.

For the measurements made with the ICCD camera, the exposure of the camera was synchronized with the chopper wheel so that each image contains either a LIF signal induced from one of the lasers or optical background (both laser beams blocked). This procedure enables online background subtraction and it compensates for slow fluctuations and drifts during the measurements, e.g., varying seeding concentrations. The sampling rate of the camera was 9 Hz resulting in an effective rate of 3 Hz per laser band and background. During each measurement 600 images were acquired, i.e., 200 per band with an exposure time of 8 ms. The LIF signal for each laser band utilized in the temperature evaluations is an average of these 200 images. When the line array camera was utilized, the signal was 400 exposures per laser band with an exposure time of 1.97 ms. The three different signals, LIF from laser one, LIF from laser two, and the background, were instead identified in the data evaluation.

3. RESULTS AND DISCUSSION

A. Line Measurements

Four different range-resolved temperature measurement series were carried out in the flame at different heights above the burner (HAB); two using the line array detector and two using the ICCD camera. The measurements were performed during different days. The total range interval monitored with the line array detector was 150–340 cm, with the burner located at 163 cm. For the measurements with the ICCD camera the range interval was 136–172 cm, and the burner was placed at 143 cm. The difference in Scheimpflug configurations

between the two cases results in different range resolution in the flame, specifically a higher resolution for the ICCD camera case. There are several factors that affect the range resolution of the Scheimpflug setup, e.g., size of the detector, width of the laser beam, and choice of range interval. This has been discussed in [10]. Assuming an infinitely narrow laser beam, the pixel resolution at the position of the burner for the line array case is 0.5 mm, while it is 0.35 mm for the ICCD. In practice, taking the width of the beam into account, the resolution is roughly estimated to be 1.7 mm and 1.4 mm, respectively.

Figure 3(a) shows the resulting LIF signals upon excitation at 410 and 451 nm, respectively, for one of the line array camera measurements at 2 mm HAB. Figure 3(b) displays the corresponding profiles acquired with the ICCD camera. The profiles of the indium fluorescence show clear peaks at the edge of the burner. This can be explained by an outer reaction zone, where decomposition of indium species and radicals increase the number of indium atoms and a higher signal is therefore obtained. This profile becomes flatter for leaner flames (i.e., flames with lower equivalence ratios). The difference in shape between the profile obtained with the ICCD camera and the profile obtained with the line array camera is due to the difference in resolution [10]. The lower resolution associated with the latter case makes the "valley" in the signal at the center of the flame shallower. The corresponding evaluated temperatures are shown in Figs. 3(c) and 3(d).

The evaluated mean temperatures in the middle of the burner, i.e., the average temperature across the flat part of the temperature profiles, for all four measurements are plotted as a function of HAB in Fig. 4. A linear interpolation between the different HABs was done for each measurement, and the solid black line displays the mean of these interpolations. The

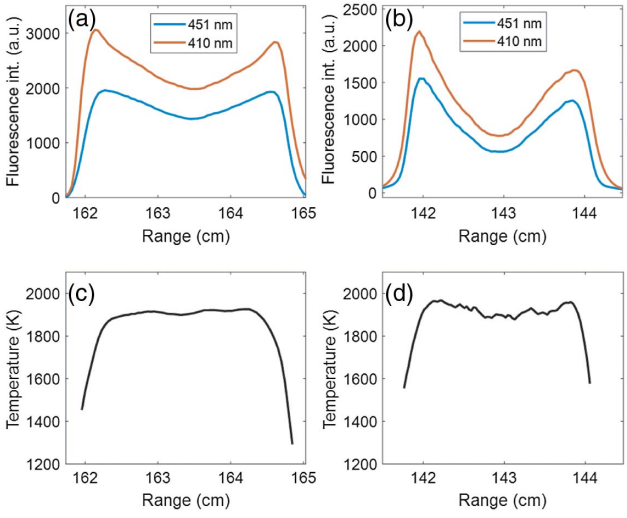

Fig. 3. (a) 451 nm fluorescence profiles for the two different excitation wavelengths at HAB of 2 mm using the line array camera. (b) Corresponding fluorescence signals using the 2D camera. (c) Evaluated temperature profile for the signals shown in (a). (d) Evaluated temperature profile for the signals shown in (b). The equivalence ratio of the methane/air flame was 1.2. The standard deviations across the plateau for the temperature curves in (c) and (d) are 11 and 25 K, respectively.

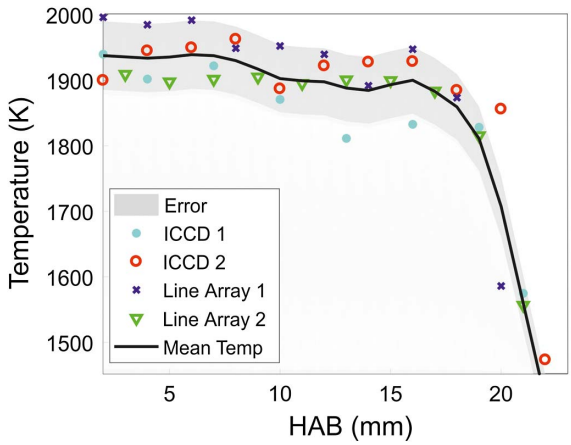

Fig. 4. Four series of temperature measurements at different HABs recorded during different days. Two of the measurements were made with the line array camera and the other two with the ICCD camera. A linear interpolation between the different HABs was performed for each series of measurements, and the solid black line displays the mean of these interpolations. The shaded area plot corresponds to the estimated accuracy of 2.7% for the technique. The equivalence ratio of the methane/air flame was 1.2.

shaded area corresponds to the estimated accuracy of 2.7% [23]. The two main sources of error are the overlap between the laser line and the absorption line, and uncertainty in the laser power measurements. We note that our temperatures measured at 3–15 mm HAB are close to the adiabatic flame temperature. This suggests that the method over-predicts the temperature to some extent, since cooling by the burner and the seeding solution should decrease the temperature.

B. 2D Measurements

2D temperature measurements were also carried out in the same flame using the ICCD camera. The laser beams were now shaped into sheets, which were focused above the center of the burner ($f = 1000$ mm). The height of the sheet was 5 mm. Since the vertical beam profile of the two laser beams are not identical this has to be compensated for. To characterize the beam profiles, reference measurements, based on elastic scattering in a homogenous flow of vaporized H_2O, were carried out for both beams (410 and 451 nm). For the reference measurement at 410 nm the bandpass filter with a center wavelength of 450 nm had to be replaced with one having a center wavelength at 410 nm. Due to chromatic aberrations and different properties of the filters, the elastic signal at 410 nm did not overlap spatially with the fluorescence signal at 451 nm. To deal with this issue, two reference images of a target with many bright dots, similar to reference targets used in particle image velocimetry, were recorded, one with the 451 nm filter in front of the camera, and one with the 410 nm filter. The position of each dot was identified for both images and a transformation function defining the difference was found. The transformation function was then used to adjust the position of the 410 nm laser profile in the image to overlap with the fluorescence signal.

Figure 5(a) displays the resulting 2D temperature profile. The vertical temperature profile in the middle of the flame

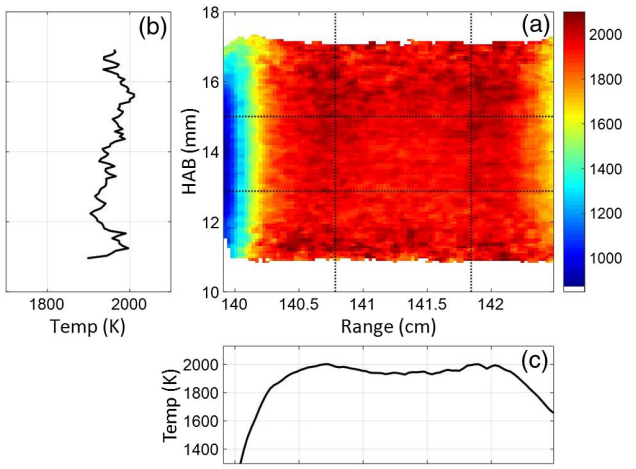

Fig. 5. Temperatures measured with TLAF in a flat flame of equivalence ratio 1.2 at a range of ∼1.41 cm. (a) 2D-temperature distribution of the flame. (b) Corresponding vertical temperature profile. The profile is the average temperature in the area marked by the vertical dotted lines in (a), i.e., range 140.8–141.8 cm. (c) Corresponding horizontal temperature profile, which is the average temperature in the area marked by the horizontal dotted lines in (a), i.e., 13–15 mm HAB.

is shown in Fig. 5(b). The result is the average temperature in the area marked by the two horizontal dotted lines in Fig. 5(a). Figure 5(c) presents the horizontal temperature profile, which is the average temperature in the area with in the dotted vertical lines. The vertical and horizontal profiles attained from the 2D image, Fig. 5(b) and 5(c), respectively, show a similar result as the 1D measurement, i.e., a temperature between 1900 and 2000 K. The vertical profile shown in Fig. 5 corresponds quite well to the flat 1D temperature profile between 12 and 17 mm HAB shown in Fig. 4.

C. Discussion

For the present measurement a lens with $f = 1000$ mm was used to focus the laser beam in the flame. The resolution of a Scheimpflug lidar measurement is affected by the shape (more specifically the width) of the laser beam [6,10]. This means that the beam shape should be adapted to the application in question. If the aim is to measure in a small probe volume from a distance it might be favorable to focus the beam in that volume, using a lens with a long focal length or a telescope, and as a result attain a high range resolution locally in the region of interest. If one instead wants to measure over a larger range interval, it might be better to use a collimated beam, having virtually the same width along the entire region of interest, at the expense of deteriorated resolution. Another alternative is to use a telescope and focus the beam at the far end of the range. The narrowing of the beam would then compensate for the intrinsic decrease in resolution due to the geometrical constraints of the Scheimpflug principle.

It was found that the reproducibility of the 2D measurements is critically dependent on the compensation for the spatial beam profiles. Small shifts of the beam profile compensation give rise to errors in the temperature evaluation. A sensitivity study, where the fluorescence image at one of the wavelengths was shifted one pixel before extracting the fluorescence ratio, resulted in a changed temperature difference between the top and bottom of the vertical temperature profile [see Fig. 5(b)] of 100 K. This kind of problem may be exacerbated by the large observation distance, since a small change in position of the signal on the camera chip results in a large shift in the probe volume. For the 2D measurements the filters had to be changed when performing reference measurements for the beam profile compensation (described in Section 3.B). It is difficult to place the filters in the exact same position every time they are moved, and this could lead to a shift in the signal that the transformation function cannot correct for. This issue may explain the difference between the 1D (Fig. 4) and 2D (Fig. 5) temperatures obtained with the ICCD camera at the same HABs. To avoid moving the filters a customized filter covering both 410 and 451 nm could possibly be used for future experiments. This would mean that the fluorescence from both 410 and 451 nm would be collected during the actual measurements and the evaluation would have to be adapted to this. Another possible way to avoid moving the filters would be to use a stereoscopic method where the fluorescence signal is split into two components, which are then detected by different parts of the detector covered by different filters [23].

4. CONCLUSION

The work presented here demonstrates that accurate single-optical-port thermometry is feasible in combustion environments by implementing the TLAF technique into a Scheimpflug lidar setup. The 1D temperature measurements in the McKenna flame result in reliable temperatures, lying within the estimated measurement error of the TLAF technique. The initial study of the capacity for 2D thermometry shows promising results, with vertical and horizontal profiles similar to those obtained in the 1D measurements, suggesting a good potential for remote single-optical-port temperature imaging. In summary, it is anticipated that the developed measurement concept could enable critical temperature information, 1D and 2D, in the most intractable conditions prevailing in many industrial applications, suffering from limited optical access.

Funding. Energimyndigheten (225383, 389131); H2020 European Research Council (ERC) (669466); Knut och Alice Wallenbergs Stiftelse (2013.0036, 2015.0294).

REFERENCES

1. B. Kaldvee, A. Ehn, J. Bood, and M. Aldén, "Development of a picosecond lidar system for large-scale combustion diagnostics," Appl. Opt. **48**, B65–B72 (2009).
2. B. Kaldvee, C. Brackmann, M. Aldén, and J. Bood, "LII-lidar: range-resolved backward picosecond laser-induced incandescence," Appl. Phys. B **115**, 111–121 (2014).
3. B. Kaldvee, C. Brackmann, M. Aldén, and J. Bood, "Highly range-resolved ammonia detection using near-field picosecond differential absorption lidar," Opt. Express **20**, 20688–20697 (2012).
4. B. Kaldvee, J. Wahlqvist, M. Jonsson, C. Brackmann, B. Andersson, P. van Hees, J. Bood, and M. Aldén, "Room-fire characterization using highly range-resolved picosecond lidar diagnostics and CFD simulations," Combust. Sci. Technol. **185**, 749–765 (2013).
5. M. Brydegaard, E. Malmqvist, S. Jansson, J. Larsson, S. Török, and G. Zhao, "The Scheimpflug lidar method," Proc. SPIE **10406**, 104060I (2017).

6. L. Mei and M. Brydegaard, "Atmospheric aerosol monitoring by an elastic Scheimpflug lidar system," Opt. Express **23**, A1613–A1628 (2015).
7. L. Mei and P. Guan, "Development of an atmospheric polarization Scheimpflug lidar system based on a time-division multiplexing scheme," Opt. Lett. **42**, 3562–3565 (2017).
8. T. Scheimpflug, "Improved method and apparatus for the systematic alteration or distortion of plane pictures and images by means of lenses and mirrors for photography and for other purposes," GB patent GB190401196A (12 May 1904).
9. J. Carpentier, "Improvements in enlarging or like cameras," GB patent 1139 (17 January 1901).
10. E. Malmqvist, M. Brydegaard, M. Aldén, and J. Bood, "Scheimpflug lidar for combustion diagnostics," Opt. Express **26**, 14842–14858 (2018).
11. R. B. Miles, W. R. Lempert, and J. N. Forkey, "Laser Rayleigh scattering review," Meas. Sci. Technol. **12**, R33–R51 (2001).
12. A. McIlroy, J. B. Jeffries, K. Kohse-Höinghaus, and J. B. Jeffries, *Applied Combustion Diagnostics* (Taylor & Francis, 2002).
13. A. Bohlin and C. J. Kliewer, "Communication: two-dimensional gas-phase coherent anti-Stokes Raman spectroscopy (2D-CARS): simultaneous planar imaging and multiplex spectroscopy in a single laser shot," J. Chem. Phys. **138**, 221101 (2013).
14. A. Bohlin, M. Mann, B. D. Patterson, A. Dreizler, and C. J. Kliewer, "Development of two-beam femtosecond/picosecond one-dimensional rotational coherent anti-Stokes Raman spectroscopy: time-resolved probing of flame wall interactions," Proc. Combust. Inst. **35**, 3723–3730 (2015).
15. S. Roy, J. R. Gord, and A. K. Patnaik, "Recent advances in coherent anti-Stokes Raman scattering spectroscopy: Fundamental developments and applications in reacting flows," Prog. Energy Combust. Sci. **36**, 280–306 (2010).
16. W. G. Bessler, F. Hildenbrand, and C. Schulz, "Two-line laser-induced fluorescence imaging of vibrational temperatures in a NO-seeded flame," Appl. Opt. **40**, 748–756 (2001).
17. R. Devillers, G. Bruneaux, and C. Schulz, "Development of a two-line OH-laser-induced fluorescence thermometry diagnostics strategy for gas-phase temperature measurements in engines," Appl. Opt. **47**, 5871–5885 (2008).
18. P. R. Medwell, Q. N. Chan, P. A. M. Kalt, Z. T. Alwahabi, B. B. Dally, and G. J. Nathan, "Development of temperature imaging using two-line atomic fluorescence," Appl. Opt. **48**, 1237–1248 (2009).
19. A. Manteghi, Y. Shoshin, N. J. Dam, and L. P. De Goey, "Two-line atomic fluorescence thermometry in the saturation regime," Appl. Phys. B **118**, 281–293 (2015).
20. I. S. Burns, X. Mercier, M. Wartel, R. S. M. Chrystie, J. Hult, and C. F. Kaminski, "A method for performing high accuracy temperature measurements in low-pressure sooting flames using two-line atomic fluorescence," Proc. Combust. Inst. **33**, 799–806 (2011).
21. J. Borggren, W. Weng, A. Hosseinnia, P.-E. Bengtsson, M. Aldén, and Z. Li, "Diode laser-based thermometry using two-line atomic fluorescence of indium and gallium," Appl. Phys. B **123**, 278 (2017).
22. T. Leffler, C. Brackmann, W. Weng, Q. Gao, M. Aldén, and Z. Li, "Experimental investigations of potassium chemistry in premixed flames," Fuel **203**, 802–810 (2017).
23. J. Borggren, W. Weng, M. Aldén, and Z. Li, "Spatially resolved temperature measurements above a burning wood pellet using diode laser-based two-line atomic fluorescence," Appl. Spectrosc. **72**, 964–970 (2017).